# Real-Time Control of a Semi-Industrial Fed-Batch Evaporative Crystallizer Using Different Direct Optimization Strategies

**Ali Mesbah**
Delft Center for Systems and Control, Delft University of Technology, 2628 CD Delft, The Netherlands

Process and Energy Laboratory, Delft University of Technology, 2628 CA Delft, The Netherlands

**Adrie E. M. Huesman**
Delft Center for Systems and Control, Delft University of Technology, 2628 CD Delft, The Netherlands

**Herman J. M. Kramer**
Process and Energy Laboratory, Delft University of Technology, 2628 CA Delft, The Netherlands

**Zoltan K. Nagy**
Dept. of Chemical Engineering, Loughborough University, LE11 3TU, U.K.

**Paul M. J. Van den Hof**
Delft Center for Systems and Control, Delft University of Technology, 2628 CD Delft, The Netherlands

*DOI 10.1002/aic.12366*
*Published online August 26, 2010 in Wiley Online Library (wileyonlinelibrary.com).*

*This article presents a model-based control approach for optimal operation of a seeded fed-batch evaporative crystallizer. Various direct optimization strategies, namely, single shooting, multiple shooting, and simultaneous strategies, are used to examine real-time implementation of the control approach on a semi-industrial crystallizer. The dynamic optimizer utilizes a nonlinear moment model for on-line computation of the optimal operating policy. An extended Luenberger-type observer is designed to enable closed-loop implementation of the dynamic optimizer. In addition, the observer estimates the unmeasured process variable, namely, the solute concentration, which is essential for the intended control application. The model-based control approach aims to maximize the batch productivity, as satisfying the product quality requirements. Optimal control of crystal growth rate is the key to fulfill this objective. This is due to the close relation of the crystal growth rate to product attributes and batch productivity. The experimental results suggest that real-time application of the control approach leads to a substantial increase, i.e., up to 30%, in the batch productivity. The reproducibility of batch runs with respect to the product crystal size distribution is achieved by thorough seeding. The simulation and experimental results indicate that the direct optimization strategies perform similarly in terms of optimal process operation. However, the single shooting strategy is computationally more expensive.* © 2010 American Institute of Chemical Engineers *AIChE J,* 57: 1557–1569, 2011

Correspondence concerning this article should be addressed to A. Mesbah at ali.mesbah@tudelft.nl.

*Keywords: batch crystallization, nonlinear moment model, seeding, model-based control, dynamic optimization, state estimation, real-time implementation*

## Introduction

Batch crystallization is widely used in the pharmaceutical, food, and fine chemical industries to produce high-value-added specialty chemicals with high purity as well as desired crystal size distribution (CSD) and shape. Despite the extensive application of batch crystallizers, their model-based control poses a significant number of challenges. The difficulties mainly arise from the nonlinear process dynamics described by distributed models, kinetic uncertainties, nonideal mixing, sensor limitations in accurately measuring the process variables, inherent process uncertainties and lack of process actuation.[1,2] Nonetheless, model-based control of batch crystallizers allows for fulfilling the stringent requirements of the consumer-driven market as well as enhancing the process productivity in the increasingly competitive pharmaceutical and chemical industries.

The operation of batch crystallizers is conventionally performed by manipulating the supersaturation trajectory. Implementation of programmed temperature profiles on batch cooling crystallizers dates back to early 1970s. The pioneering work of Mullin and Nyvlt[3] as well as Jones and Mullin[4] established that a programmed cooling profile leads to a better CSD characteristics in comparison with uncontrolled or linear cooling policies. Mayrhofer and Nyvlt[5] analyzed programmed cooling of batch crystallizers on the basis of a moment model. They devised a theoretical cooling profile with an arbitrary ratio of seeding to spontaneous nucleation that could be simplified to the previously reported expressions. Early on, optimal control theory was also used to determine cooling policies. Jones[6] used the maximum principle to compute a cooling profile that maximized final size of the seed crystals. Chang and Epstein[7] applied a gradient method to determine the optimal temperature profiles for various objective functions expressed in terms of average size, volume, or variance of the final CSD.

Over the past decade, dynamic optimization of batch crystallizers has received particular attention. Dynamic optimization exploits a process model to systematically push the batch process to its most optimal operating regime, whereas honoring various operational and product quality requirements. The explicit formulation of constraints in a dynamic optimization problem facilitates optimal process operation realized at the constraints. In addition, inclusion of constraints into the control problem offers flexibility in the process operation.

Producing a crystalline material with a large mean crystal size and a narrow size distribution is traditionally the prime objective in the control of batch crystallizers.[8] Matthews and Rawlings[9] identified a model for batch cooling crystallization of an organic photochemical-heptane system. Model parameter uncertainties were minimized by applying different optimal experimental design techniques. Open-loop optimization of the temperature profile was performed to improve filtration properties of the crystallization slurry. Lang et al.[10] computed the optimal programmed cooling curve of an industrial batch cooling crystallizer by solving a dynamic optimization problem, which maximized the final crystal size. The optimal temperature profile led to a drastic increase in the mean crystal size as compared to the operating policy obtained by the maximum principle optimization and the original operating conditions determined by trial and error. Chung et al.[11] performed a comprehensive study on dynamic optimization of the seed distribution in a batch cooling crystallizer. Certain properties of the product crystals were optimized over the supersaturation profile and the seed characteristics. It was shown that optimizing over the seed distribution could have a larger effect on the product than optimizing over the supersaturation profile. The latter study was extended by Ma et al.[12] to quantify the impact of parameter and control implementation inaccuracies on the performance of open-loop control policies. In addition, Ma et al.[13] investigated the optimal control of batch formation of multidimensional crystals. They showed that a subtle change in the optimal control objective could have a significant impact on crystal size and shape distributions of the product crystals. Later on, Nagy and Braatz[14] underlined the high sensitivity of optimal control trajectories to model uncertainties. They presented a new approach for incorporating robustness in the model-based control of batch crystallization processes. Optimal control of batch cooling crystallizers was also studied by Hu et al.[15] They proposed a new method for numerical solution of the population balance equation. The system-specific kinetic parameters of the crystallizing system were estimated on the basis of the maximum likelihood method. The identified model was used to determine an optimal cooling policy by minimizing the ratio of the mass of the newly nucleated crystals to the seed crystals. Experimental results indicated that the optimal temperature profile led to improved operation of the crystallizer in comparison with uncontrolled and linear cooling policies. Nowee et al.[16] presented a model for a seeded cooling crystallization process, in which crystal dissolution took place. The nonlinear process model was used to optimize the temperature profile and the initial seed size distribution. Experimental implementation of the off-line optimized profiles resulted in the desired crystal mean size.

Despite the significant efforts to develop model-based control approaches for seeded batch crystallizers, a great deal of the work is limited to open-loop control as discussed above. The main shortcomings of the latter control approach are its insensitivity to batch-to-batch variations arisen from uncertain initial seeding as well as its inability to cope with process uncertainties. In addition, the models used to devise optimal operating policies often provide an incomplete description of the process. This is mainly due to the uncertainties associated with the kinetic expressions.

An effective approach that alleviates the shortcomings of open-loop control is on-line computation of the optimal operating policy during a batch run. In the so-called closed-loop control approach, a feedback mechanism is exploited to update the optimal operating policy by using information from the process, i.e., measurements. The feedback mechanism is essential to reject process disturbances and to account for model imperfections.

Among the numerous attempts to perform closed-loop control of batch crystallizers, the work of Chang and Epstein[17] can be recognized as a pioneering study. They proposed a strategy for incorporating feedback into the optimal control scheme presented in their earlier work.[7] The application of the feedback control strategy for batch crystallizers was demonstrated by simulation studies. Eaton and Rawlings[18] investigated feedback control of several constrained nonlinear multivariable chemical processes, including a batch cooling crystallizer, using nonlinear estimation and optimal control strategies. Zhang and Rohani[19] developed an on-line control strategy for optimal quality control of a seeded batch cooling crystallizer. An extended Kalman filter was used to estimate the unmeasured state variables and to account for plant-model mismatch as well as process uncertainties. The simulation results showed notable improvements in the product CSD in comparison with that obtained by open-loop implementation of the optimal cooling policy.

In recent years, the advent of process analytical technology (PAT) and the ever growing computing power have significantly facilitated real-time implementation of closed-loop control approaches. Abbas and Romagnoli[20] presented a model-based control approach consisting of advanced modeling software, a linear model predictive controller, and a soft-sensor. At the top layer of the control hierarchy, dynamic optimization was used to determine the off-line optimal mean crystal size, which became the set point for the lower layer real-time optimizer. The feedback mechanism was introduced at the latter layer through a soft sensor that inferred the mean crystal size on the basis of temperature and conductivity measurements. The control approach was tested on a 75-l batch cooling crystallizer. The experimental results showed a rather successful set point tracking toward the batch end. Sheikhzadeh et al.[21] used an in-situ FBRM probe in combination with ATR-FTIR spectroscopy to provide on-line measurements of crystallization kinetics and solute concentration. The measurements were used in a feedback fashion to update the optimal operating policy at each optimization time interval. They investigated the effect of single- and multi-objective optimal control on the properties of crystals produced in a bench scale semi-batch anti-solvent crystallizer. The experimental results demonstrated that the multi-objective optimization led to better size distribution properties of the product crystals. Landlust et al.[22] presented an industrial model predictive control approach for batch crystallization processes. The control approach consisted of a model predictive controller, an observer, and a nonlinear moment model. To use the nonlinear model in the model predictive controller, the moment model was locally linearized along the operating trajectory. Real-time implementation of the control approach on a semi-industrial fed-batch evaporative crystallizer resulted in a notable increase in the process productivity, as the desired properties of the product crystals were obtained. Recently, Nagy[23] proposed a robust control methodology to achieve the desired shape of CSD. The approach combined the concepts of model-free direct design[24] and model-based control in a hierarchical framework. The optimizer used concentration, temperature, and chord length distribution measurements to repeatedly compute the optimal supersaturation profile. The latter profile was then applied as the set point for the supersaturation controller. The concentration and chord length distribution measurements were performed by using an ATR-UV spectrometer and an FBRM probe, respectively. Real-time implementation of the control approach on a bench scale cooling crystallizer showed that the target CSD could be achieved even in the case of a sudden change in the nucleation rate.

In almost all of the aforementioned studies, the dynamic optimization problem was solved using the direct single shooting optimization strategy. However, the single shooting strategy is expected to render real-time optimization of industrial batch crystallizers computationally infeasible. This is due to the large number of state variables of the population balance models that may result in excessive computational burden of the dynamic optimizer. This article primarily intends to investigate how the choice of the direct optimization strategy influences closed-loop control of crystallization processes. Various direct optimization strategies, namely, single shooting, multiple shooting, and simultaneous strategies, are used to examine real-time viability of optimal operation of a semi-industrial batch crystallizer. The performance, computational requirements, and implementation-related issues of the direct optimization strategies are thoroughly investigated by several simulation and experimental studies.

A model-based control approach is presented for optimal operation of a semi-industrial seeded fed-batch evaporative crystallizer. The underlying optimal control problem is solved by using single shooting, multiple shooting, and simultaneous optimization strategies. The control approach aims to optimally operate the batch crystallizer within the metastable zone by manipulating the supersaturation. This allows us to maximize the production capacity, as fulfilling the product quality requirements. An extended Luenberger observer is designed to facilitate closed-loop implementation of the control approach. The observer also enables estimation of the unmeasured process variable, namely, the solute concentration, that is essential for the intended control application. The real-time viability of the control approach is demonstrated by several closed-loop implementations on a semi-industrial crystallizer.

## Process Description

The real-time feasibility of the model-based control approach is experimentally investigated for fed-batch evaporative crystallization of an ammonium sulfate-water system. As shown in Figure 1, crystallization takes place in a 75-l draft tube crystallizer equipped with a distributed control system (DCS CENTUM CS3000, Yokogawa, Japan). The crystallizer is considered as a single well-mixed compartment with one inlet and two outlet streams. The evaporative crystallization is carried out isothermally at 50°C. The fed-batch operation is exercised to compensate for losses in the crystallization volume due to the evaporation of solvent, i.e., water, and slurry sampling. Thus, the crystallizer is continuously fed throughout a batch run with a crystal-free feed stream containing saturated ammonium sulphate solution. The outlet flows from the crystallizer include an unclassified product removal stream as well as a vapor stream that is free from crystal and solute. The small product flow is

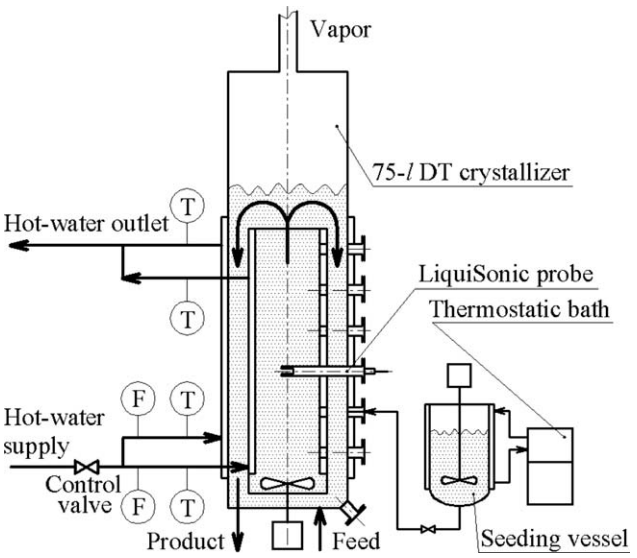


**Figure 1. The 75-l draft tube crystallizer.**

withdrawn from the crystallizer at regular time intervals every 100 s. The product flow is diluted with the saturated feed solution for 20 s to facilitate on-line measurement of CSD with a laser diffraction instrument (HELOS-Vario, Sympatec, Germany).

To ensure the reproducibility of batch runs and the achievement of desired product specifications, seeding is carried out. Ground seeds are prepared by milling and sieving of the commercial product crystals of ammonium sulphate (DSM, The Netherlands) to collect 0.6 kg of the 90–125 $\mu$m sieve fraction. Before insertion into the crystallizer, the seed crystals are aged for one hour in a saturated solution of ammonium sulphate at 50°C.[25] An in-line concentration measuring probe (LiquiSonic, SensoTech, Germany) is used to detect the predetermined supersaturation, at which the seeds are introduced to the vessel.

## Crystallization Model

The cornerstone of any model-based control approach is its dynamic process model, describing the dynamic relation between the relevant inputs and outputs of the system to be controlled. These control approaches use the model to continuously explore the degrees of freedom in the process to achieve the desired performance in accordance with an optimization criterion.

The dynamic behavior of a solution crystallization process can be described by the population balance equation, along with the conservation balance equations and kinetic relations. The population balance equation accounts for the evolution of number of crystals along temporal and size domains. Under the assumptions of well-mixed suspension, constant crystallizer volume, size-independent growth of crystals, nucleation of crystals of infinitesimal size, and negligible breakage and agglomeration, the dynamic population balance equation for the fed-batch crystallizer is expressed as[26]

$$\frac{\partial n(L,t)}{\partial t} = -G(t)\frac{\partial n(L,t)}{\partial L} - \frac{Q_p}{V}n(L,t) \tag{1}$$

with the left boundary condition

$$n(L_0,t) = \frac{B_0(t)}{G(t)|_{L_0}}. \tag{2}$$

In Eq. 1 $n$ is the number density function (#m$^{-3}$ m$^{-1}$), $G$ is the crystal growth rate (m s$^{-1}$), $B_0$ is the total nucleation rate (#m$^{-3}$ s$^{-1}$), $t$ is the time (s), $L$ is the characteristic crystal size (m), $V$ is the crystallizer volume (m$^3$), and $Q_p$ is the unclassified product removal flow rate (m$^3$ s$^{-1}$).

The population balance equation is a hyperbolic partial differential equation, whose solution is typically obtained by approximating the original equation with a finite number of ordinary differential equations. This is done by discretizing the crystal size distribution. Accurate numerical solution of the population balance equation often requires a large number of discretization points, which may render dynamic optimization computationally too expensive for real-time implementations. Thus, the method of moments[27] is applied to Eq. 1 to recast the population balance equation into a set of computationally affordable ordinary differential equations. The method of moments essentially calculates properties of the total crystal population that are required for the intended control application. Upon multiplying both sides of Eq. 1 by $L^i dL$ and integrating over the entire crystal size domain, the following set of ordinary differential equations is obtained

$$\frac{dm_i}{dt} = 0^i B_0 + iGm_{i-1} - \frac{m_i Q_p}{V} \qquad m_i(t_0) = m_{i,0} \qquad i = 0,\ldots,4. \tag{3}$$

Eq. 3 describes the evolution of the moments of CSD in time.

The particle formation is attributed to secondary nucleation from crystal surfaces because it is often the most dominant nucleation mechanism occurring in seeded batch crystallizers. The empirical expressions realized for the total nucleation rate and the size-independent crystal growth rate are[28]

$$B_0 = k_b m_3 G \tag{4}$$

$$G = k_g (C - C^*)^g. \tag{5}$$

The nucleation rate constant $k_b$, the growth rate constant $k_g$, and the growth rate exponent $g$ are the kinetic parameters that should be estimated. Furthermore, $C$ and $C^*$ are the solute concentration and the saturation concentration, respectively, whose difference determines the driving force, namely the supersaturation, of the crystallization process.

Because of the isothermal operation of the evaporative crystallizer at hand, the mass and energy balance equations simplify to a single expression for the solute concentration

$$\frac{dC}{dt} = \frac{\frac{Q_p(C^*-C)}{V} + 3K_v G m_2 (k_1 + C)}{1 - K_v m_3} + \frac{k_2 H_{in}}{1 - K_v m_3} \qquad C(t_0) = C_0 \tag{6}$$

with the constant coefficients

**Table 1. Model Parameters and Physical Properties of the Ammonium Sulphate-Water Crystallizing System**

| Parameter | Value |
|---|---|
| $C^*$, ($kg_{solute}/kg_{solution}$) | 0.46 |
| $H_c$, (kJ/kg) | 60.75 |
| $H_L$, (kJ/kg) | 69.86 |
| $H_v$, (kJ/kg) | $2.59 \times 10^3$ |
| $K_v$ | 0.43 |
| $k_b$, (#/m$^4$) | $7.82 \times 10^{14}$ |
| $k_g$, (m/s) | $4.91 \times 10^{-5}$ |
| $Q_p$, (m$^3$/s) | $1.73 \times 10^{-6}$ |
| $V$, (m$^3$) | $7.50 \times 10^{-2}$ |
| $\rho_c$, (kg/m$^3$) | 1767.35 |
| $\rho_L$, (kg/m$^3$) | 1248.93 |

$$k_1 = \frac{H_v C^*}{H_v - H_L}\left(\frac{\rho_c}{\rho_L} - 1 + \frac{\rho_L H_L - \rho_c H_c}{\rho_L H_v}\right) - \frac{\rho_c}{\rho_L} \tag{7}$$

$$k_2 = \frac{C^*}{V\rho_L(H_v - H_L)}, \tag{8}$$

where $K_v$ is the crystal volumetric shape factor, $H_{in}$ is the heat input to the crystallizer (kW), $\rho_L$ is the density of saturated solution (kg m$^{-3}$), and $\rho_c$ is the density of crystals (kg m$^{-3}$). $H_L$, $H_c$, and $H_v$ are the solution, crystal, and vapor specific enthalpies (kJ kg$^{-1}$), respectively.

From the aforementioned analysis, it follows that the dynamics of the seeded batch crystallizer are described by a set of nonlinear differential algebraic equations of the general form

$$\begin{aligned} \dot{x} &= f(t, x, z, y, u, \theta) \qquad x(t_0) = x_0 \\ 0 &= g(t, x, z, y, u, \theta) \\ y &= h(t, x, z, y, u, \theta), \end{aligned} \tag{9}$$

where $f$, $g$, and $h$ are the set of explicit model state, algebraic, and output equations, respectively, $x$ is the state vector containing the five leading moments of CSD and the solute concentration, $z$ is the vector of algebraic variables, i.e., $B_0$ and $G$, $y$ is the vector of process outputs consisting of the five leading moments of CSD, $u$ is the process input, namely the heat input to the crystallizer, and $\theta$ is the model parameter set. Note that $x_0$ represents the initial states of the system determined by the seed characteristics and the initial solute concentration. The model parameters and physical properties of the ammonium sulfate-water crystallizing system are listed in Table 1.

Mesbah et al.[29] demonstrated that the moment model provides an adequate description of the process. This is due to the optimal seeding procedure used in batch runs to minimize the secondary nucleation and as a result narrow the operational envelop. Owing to the large seed loads, the dynamic evolution of crystal size distribution is mainly governed by the crystal growth rate.[30] Hence, the CSD is expected to be unimodal and therefore can be well represented by the mean crystal size and the CSD width obtained from the moment model.

## On-Line Model-Based Control Approach

### *Dynamic optimization*

The approach to be used for optimal operation of a crystallization process is largely dependent on the required product specifications and the properties of the crystallizing system. In batch crystallizers, growth dominant operation is often preferred since the crystal growth rate is a key process variable closely related to product characteristics and batch productivity. Excessive crystal growth rates may, however, adversely affect the product quality due to increased impurity uptake, increased liquid inclusions as well as undesirable attrition and/or agglomeration. High-crystal growth rates can be suppressed by restraining supersaturation within the metastable zone. Hence, accurate determination of the metastable zone is essential for effective control of crystal growth rate. Experimental identification of the metastable zone can be performed by the state-of-the-art PAT tools, e.g., vibrational spectroscopy,[31] bulk video imaging,[32,33] etc.

To seek a trade off between the achievement of the desired product attributes and the maximization of batch productivity, the control objective is posed as an optimal control problem. Dynamic optimization allows us to trade off various operational and product quality requirements by imposing constraints on process inputs and outputs. The hierarchical control approach depicted in Figure 2 is used to facilitate real-time dynamic optimization of the semi-industrial batch crystallizer. The core component of the on-line control approach is an optimal control problem formulated as

$$\begin{aligned} \min_{H_{in}(t)} \quad & \frac{\int_0^{t_f} \left(100\frac{G(t)-G_{max}}{G_{max}}\right)^2 dt}{\int_0^{t_f} dt} \\ \text{s.t.} \quad & \text{Eq. 9} \\ & H_{min} \le H_{in}(t) \le H_{max}, \end{aligned} \tag{10}$$

where $H_{in}$ is the parameterized heat input profile, $t_f$ is the batch time, and $G_{max}$ is the maximum admissible crystal growth rate that circumvents detrimental effects of high supersaturation on the product quality. In Eq. 10, the heat input is the manipulated variable used to optimize the crystal growth rate profile and consequently control the supersaturation. A preceding study[34] on the controllability analysis of the crystallizer revealed that the product CSD could be hardly controlled by the available process actuators, namely, the heat input and the impeller frequency. Therefore, seeding is exercised to attain the desired product CSD attributes as well as a crystal growth dominant operational envelop, in which the crystallization phenomena are most sensitive to the heat input. The lower heat input bound $H_{min}$ is to ensure the survival of seeds at the beginning of a batch run, whereas the upper heat input bound $H_{max}$ is due to heat transfer limitations of the process. Clearly, Eq. 10 maximizes the batch productivity by attaining a maximum admissible crystal growth rate throughout the batch run. The desired product CSD attributes are achieved by the optimal seeding.

In the model-based control approach, the optimal control problem is continuously solved on-line in a receding horizon mode.[35] The principal idea of the receding horizon control algorithm is illustrated in Figure 3. At each time instant $t$, Eq. 10 is solved over the control horizon $[t\ t + T_C]$ such that the deviations of the predicted process output $y(\cdot)$ from its reference trajectory are minimized over the prediction horizon $[t\ t + T_P]$. The first element of the parameterized optimal input profile $u(\cdot)$ is then implemented on the process using a conventional proportional integral derivative (PID)

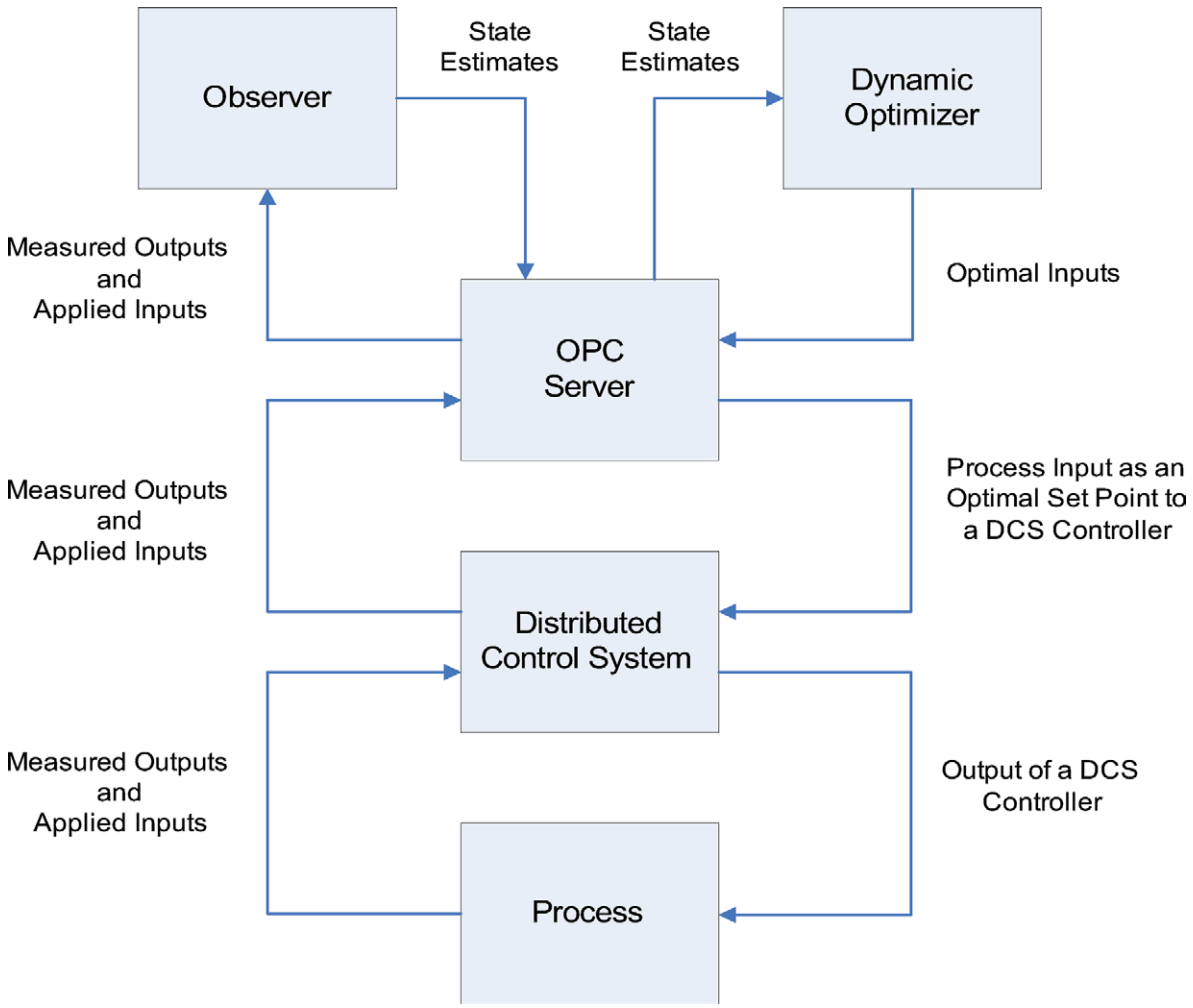


**Figure 2. The model-based control approach.**

[Color figure can be viewed in the online issue, which is available at wileyonlinelibrary.com.]

controller. The latter controller is embedded in the DCS, which forms the lowest control layer. When new on-line measurements become available, the prediction horizon shifts one sample ahead and the procedure is repeated at time instant $t + \delta$.

To recursively initialize the dynamic optimizer at each sampling time instant, an observer is required to estimate the state variables. The observer utilizes the process model and the available on-line measurements to construct the state profiles. The state estimation in combination with the feedback structure of the control approach accounts for model imperfections and process uncertainties to a large extent. In addition, the observer enables estimation of process variables, e.g., solute concentration, that may not be measured on-line due to various technological and economical limitations. The timed signal exchange among different components of the control approach is facilitated by an OPC (OLE—object linking and embedding—for process control) communication interface (IPCOS, The Netherlands).

The viability of the model-based control approach for real-time applications largely relies on efficient solution of

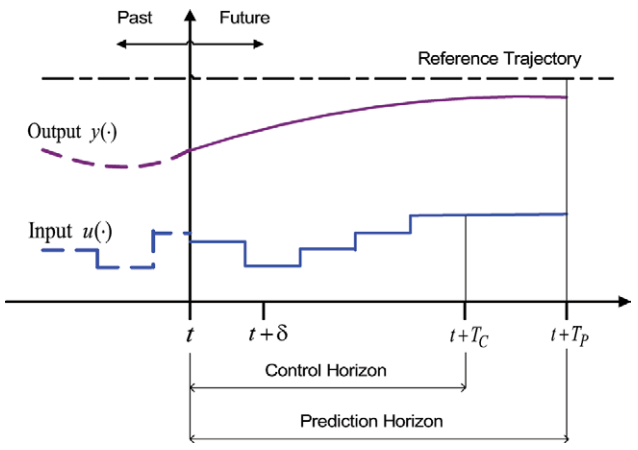


**Figure 3. Receding horizon principle.**

[Color figure can be viewed in the online issue, which is available at wileyonlinelibrary.com.]

the optimal control problem. Different direct optimization strategies, namely, single shooting, multiple shooting, and simultaneous strategies, are used to solve the dynamic optimization problem. These strategies essentially convert the original infinite dimensional optimal control problem given in Eq. 10 into a finite dimensional nonlinear programming problem (NLP). The direct optimization strategies mainly differ in whether the simulation and optimization of the resulting NLP problem are performed sequentially or simultaneously.

In the single shooting strategy,[36] the infinitely many degrees of freedom of the control vector are reduced by its parameterization. An initial value problem encompassing the model equations is numerically solved in each iteration step of the optimization procedure. The solution is obtained with high accuracy for the current values of the parameterized control vector. Thus, the model simulation and optimization are carried out sequentially, guaranteeing the solution feasibility even in the case of premature optimization terminations. On the other hand, the model equations are discretized along with the control vector in the simultaneous strategy.[37] The discretized model equations are included in the optimization problem as nonlinear constraints, typically leading to very large NLP problems. Simultaneous model simulation and optimization potentially results in faster computations in comparison with the single shooting strategy. However, feasible state trajectories are obtained merely after successful termination of the optimization as the discretized model equations are violated during the optimization procedure.

Contrary to the above discussed optimization strategies, the model simulation and optimization are not performed entirely sequentially nor simultaneously in the multiple shooting strategy.[38,39] In this strategy, the state trajectories and the control vector are parameterized over a predetermined number of intervals. The initial value problems are separately solved with a prespecified numerical accuracy on each multiple shooting interval, rendering the technique well suited for parallel computations. The relatively large number of variables necessitates the use of tailored NLP algorithms, which exploit the special structure of the problem, e.g., sparsity, to yield faster convergence than for the single shooting strategy. However, the continuity of state trajectories is only fulfilled after successful termination of the optimization procedure as with the simultaneous technique. Note that in the direct optimization strategies, the state and end point constraints are violated at premature optimization terminations.

The single shooting optimizer is implemented in Matlab, where the set of model equations and the NLP problem are sequentially solved by using the ODE15s and fmincon functions, respectively. The ODE15s solver is chosen due to its ability to efficiently integrate the set of highly stiff differential algebraic equations given in Eq. 9. The fmincon uses a sequential quadratic programming algorithm to solve medium-scale optimization problems subject to inequality constraints. The GAMS algebraic programming environment, in conjunction with the CONOPT3 solver, is used to devise the simultaneous dynamic optimizer. CONOPT3 uses a combination of various NLP algorithms, namely, sequential linear programming, generalized reduced gradient, and sequential quadratic programming algorithms. This makes CONOPT3 well suited for solving constrained optimization problems. Because of its unconditional numerical stability, the implicit Euler discretization scheme is used in the simultaneous optimizer to transform the differential equations into algebraic equations.[40] The multiple shooting optimizer is implemented in the Matlab toolbox OptCon,[41–43] which uses the large-scale nonlinear optimization solver HQP.[44] The sets of differential algebraic equations on different multiple shooting intervals are solved in parallel by using the well-known DASPK solver.[45]

### *State estimation*

An observer is devised to facilitate closed-loop implementation of the dynamic optimizer. Various state estimation techniques, e.g., extended Kalman filtering,[19] unscented Kalman filtering,[46] and moving horizon estimation[23] have been applied for output feedback control of crystallization processes. In this work, the extended Luenberger state estimation technique is used to develop a high gain nonlinear observer.[47] The merits of this estimation technique lie in its ease of implementation and low-computational burden. For the system at hand, Kalbasenka et al.[48] demonstrated that the extended Luenberger observer outperforms an extended Kalman filter with fixed process noise covariance matrix. It was shown that the deterministic estimation framework of the extended Luenberger observer could adequately cope with the disturbances acting on the process.

To design the observer, the nonlinear moment model described by Eq. 9 in its most general form is recast into

$$\begin{aligned} &\frac{dx(t)}{dt} = \mathcal{F}(x(t)) + \mathcal{G}(x(t))u(t) \qquad x(t_0) = x_0 \\ &y(t) = \mathcal{H}(x(t)), \end{aligned} \tag{11}$$

where the state vector $x(t) \in \Re^{n_x}$, the output vector $y(t) \in \Re^{n_y}$ and the input vector $u(t) \in \Re^{n_u}$ are defined as

$$\begin{aligned} x(t) &= [m_0 \quad m_1 \quad m_2 \quad m_3 \quad m_4 \quad C]^T \\ y(t) &= [m_0 \quad m_1 \quad m_2 \quad m_3 \quad m_4]^T \\ u(t) &= H_{in}. \end{aligned} \tag{12}$$

$\mathcal{F}(x(t))$ and $\mathcal{G}(x(t))$ are real-valued vector fields, whereas $\mathcal{H}(x(t))$ is a real-valued function.

The high-gain extended Luenberger-type observer is formulated as[47]

$$\frac{d\hat{x}(t)}{dt} = \mathcal{F}(\hat{x}(t)) + \mathcal{G}(\hat{x}(t))u(t) + [O(\hat{x}(t))]^{-1}KE(t) \quad \hat{x}(t_0) = \hat{x}_0, \tag{13}$$

where $\hat{x}(t)$ is the estimated state vector, $O(\hat{x}(t))$ is the observability matrix, $K$ is the finite gain vector of the observer determined by tuning, and $E(t)$ is the difference between the measured and the estimated outputs, i.e., error signal,

$$E(t) = y(t) - \mathcal{H}(\hat{x}(t)). \tag{14}$$

The structure of the gain vector is identified from a physical insight into the process. Hence, the observer tuning is

Table 2. Values of the Scaling Factors and the Optimization Parameters in Eq. 17

| Parameter | Index 1 | 2 | 3 | 4 | 5 |
|---|---|---|---|---|---|
| $a_i$ | $1 \times 10^{-10}$ | $1 \times 10^{-6}$ | $1 \times 10^{-2}$ | $1 \times 10^{2}$ | $1 \times 10^{5}$ |
| $K_i$ | $2.72 \times 10^{-3}$ | $8.45 \times 10^{1}$ | $1.17 \times 10^{-1}$ | $4.41 \times 10^{-1}$ | $4.64 \times 10^{-1}$ |

performed on the basis of a slightly different formulation of Eq. 13

$$\frac{d\hat{x}(t)}{dt} = \mathcal{F}(\hat{x}(t)) + \mathcal{G}(\hat{x}(t))u(t) + \hat{K}E(t) \qquad \hat{x}(t_0) = \hat{x}_0, \quad (15)$$

where $\hat{K} \in \Re^{n_x \times n_y}$ is a constant matrix

$$\hat{K} = \begin{bmatrix} 0 & 0 & 0 & K_1 & 0 \\ 0 & 0 & 0 & 0 & K_2 \\ 0 & 0 & K_3 & 0 & 0 \\ 0 & 0 & 0 & K_4 & 0 \\ 0 & 0 & 0 & 0 & K_5 \\ 0 & 0 & 0 & 0 & 0 \end{bmatrix}. \quad (16)$$

The entries of the last row in the above matrix are zero as the solute concentration cannot be measured in batch runs and, therefore, its corresponding error signal is not available. To circumvent initialization failure of the dynamic optimizer due to unreliable measurements for the first two moments of CSD,[29] moments $m_0$ and $m_1$ are updated by error signals of moments $m_3$ and $m_4$, respectively.

The evolution of the estimated state variables is examined by running the observer in an open-loop fashion. The entries in matrix $\hat{K}$ are determined as a solution of the following optimization problem

$$\min_{K_i} \quad \sum_{i=1}^{n_y} a_i \frac{\int_0^{t_f} |x_i(t) - \hat{x}_i(t)|\, dt}{\int_0^{t_f} dt} \quad (17)$$
$$\text{s.t.} \quad \text{Eq. 15}$$

that was formulated in gPROMS (PSE, UK). Numerical values of the scaling constants $a_i$, which account for the greatly differing orders of magnitude of the state variables, and the entries of matrix $\hat{K}$ are given in Table 2. Kalbasenka et al.[48] showed that the high-gain observer has low-estimation errors and fast convergence properties.

## Results and Discussion

### *Simulation results*

The model-based control approach is applied to a plant simulator, which simulates the process by using exactly the same moment model as the one incorporated in the controller. The initial conditions, namely, the five leading moments of the initial CSD and the initial solute concentration, of the plant model and the controller's model are identical.

Figure 4 demonstrates the simulation results of the control approach when applied to the plant simulator. As can be seen, the optimizers manipulate the heat input to the crystallizer such that the crystal growth rate is kept at its maximum admissible value, i.e., $G_{\max} = 2.5 \times 10^{-8}$ m/s; see Figure 4b. $G_{\max}$ is a conservatively chosen maximum crystal growth rate to avoid the formation of irregularly shaped crystals and to limit the undesirable effects of high supersaturation. It is observed that the maximum crystal growth rate cannot be followed at all times during a batch run as the heat input is constrained.

As expected, the three dynamic optimizers perform similarly in terms of optimal operation of the crystallizer. However, the optimization strategies have different computational burdens under approximately the same optimization settings listed in Table 3. The settings of the simultaneous strategy cannot be defined entirely identical to those of the other

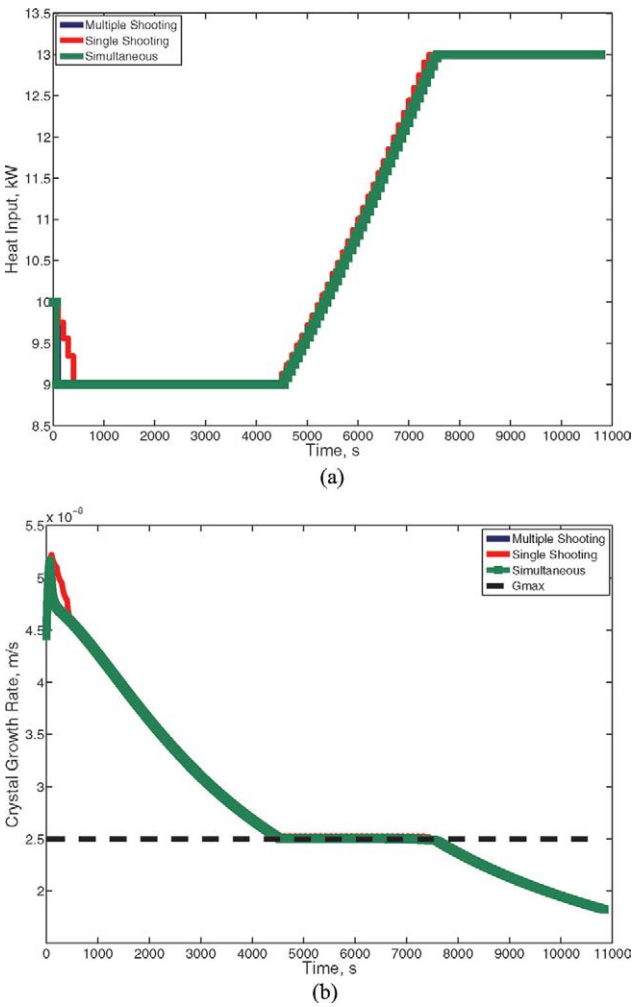


**Figure 4. Simulation results of the model-based control approach.**

(a) Heat input profiles and (b) crystal growth rate profiles. [Color figure can be viewed in the online issue, which is available at wileyonlinelibrary.com.]

**Table 3. Settings of the Dynamic Optimizers Applied to the Plant Simulator**

| | Optimization Strategy | | |
|---|---|---|---|
| | Multiple Shooting | Single Shooting | Simultaneous |
| Control horizon | 1050 s | 1000 s | 1000 s |
| Control vector parameterization* | 15 elements | 15 elements | 15 elements |
| Maximum number of QP iterations | 20 | 20 | Not applicable |
| Integration tolerance | $1 \times 10^{-6}$ | $1 \times 10^{-6}$ | Not applicable |

*Piecewise constant parameterization.

strategies. This is due to elimination of the integration solver through discretization of the model equations. The numerical efficiency of the direct optimization strategies appeared to be largely dependent on the complexity of the control vector parameterization and the scaling of the state variables. The CPU-time profiles of the dynamic optimizers over a batch run of 10,800 s are depicted in Figure 5. The single shooting strategy is the most computationally expensive optimization strategy, whereas the multiple shooting and the simultaneous strategies exhibit a much higher computational efficiency. The elimination of the model integration step in the simultaneous strategy drastically improves its numerical efficiency. However, this is achieved at the expense of handling a much larger NLP problem in comparison with the other strategies. The multiple shooting strategy has the highest efficiency owing to parallel integration of the model equations as well as exploiting the sparse structure of the NLP problem. In addition, the use of the compiled C++ model and solver libraries in the OptCon toolbox significantly improves the computational efficiency of the multiple shooting optimizer. Table 4 lists the CPU-times of the optimization strategies. It is evident that real-time implementation of the control approach is computationally viable as the maximum CPU-time during a complete optimization cycle along a batch run is considerably less than the measurement sampling time, i.e., 100 s.

### *Experimental results*

The real-time performance of the model-based control approach is evaluated by several implementations on the semi-industrial crystallizer. Variations of the crystal growth rate are examined in relation to different heat input profiles. The crystal growth rate largely affects the product quality of the seeded batch runs, whereas the heat input serves as the only driving force for supersaturation generation in the evaporative crystallizer.

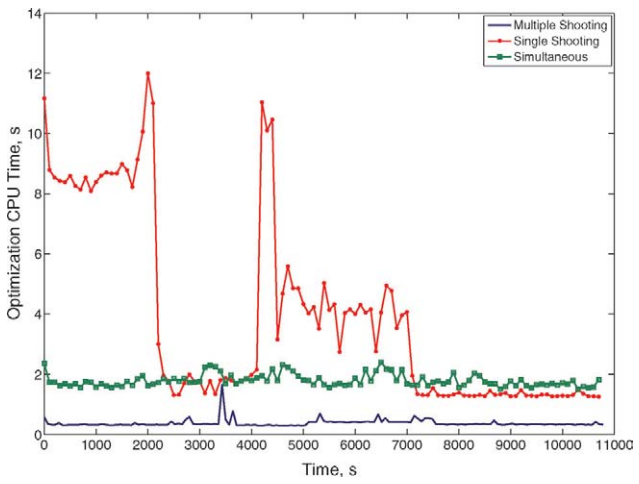


**Figure 5. CPU-time profiles.**

[Color figure can be viewed in the online issue, which is available at wileyonlinelibrary.com.]

Figure 6 depicts the heat input and the crystal growth rate profiles of various seeded batch runs, whose settings are given in Table 5. In experiment $DT_c31$, the heat input to the crystallizer is kept constant at 9 kW. As a result, the crystal growth rate gradually decays, being unable to follow its maximum admissible value; see Figure 6b. The inability to realize the maximum crystal growth rate necessitates the use of the model-based control approach. The controller should systematically push the process to its optimal operating regime, as the operational limitations are honored. In experiment $DT_c55$, open-loop implementation of the control approach is attempted. In this batch run, the optimal heat input profile is computed off-line and manually applied to the crystallizer as a time-varying set point of a PI controller. Figure 6b indicates that the crystal growth rate yet again fails to track its reference trajectory.

In experiments $DT_c63$ and $DT_c80$, the control approach is implemented in a closed-loop fashion in order to more effectively fulfill the control objective. Once the crystal growth rate crosses the reference trajectory, i.e., $G_{max}$, the heat input is raised to facilitate tighter tracking of the maximum crystal growth rate; see Figure 6. However, the reference trajectory can no longer be closely followed when the heat input reaches its upper bound. Thereafter, the crystal growth rate steadily decreases, while the heat input remains at 13 kW.

As expected, closed-loop implementation of the control approach outperforms open-loop control. The improved performance is due to the feedback of the system states. The receding horizon implementation of the dynamic optimizer not only accounts for model imperfections, but also enables effective disturbance handling through state estimation. Figure 6b suggests that the simultaneous dynamic optimizer is able to more closely follow the reference trajectory as compared to the single shooting dynamic optimizer. The

**Table 4. Computation Times of the Dynamic Optimizers Corresponding to Simulation of a Batch Run of 10800 s**

| | Total CPU-Time* over the Batch (s) | Maximum CPU-Time per Iteration (s) |
|---|---|---|
| Multiple shooting | 58.97 | 1.66 |
| Single shooting | 424.03 | 11.97 |
| Simultaneous | 194.03 | 2.39 |

*The reported CPU-times correspond to the Microsoft Windows XP (Professional) operating system running on a Genuine Intel(R) T2050 @1.60 GHz processor with 1 GB RAM.

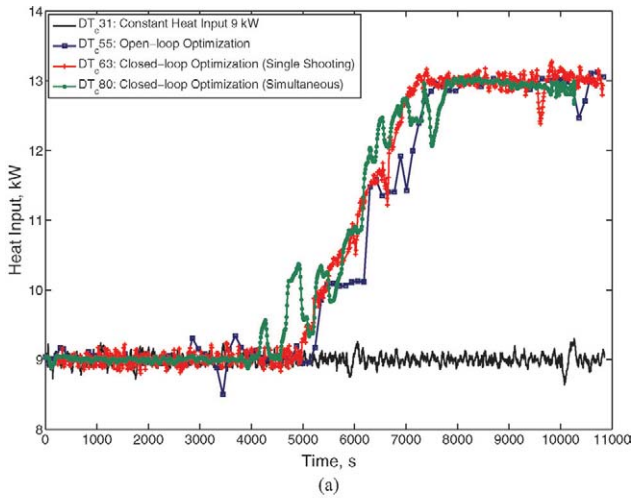


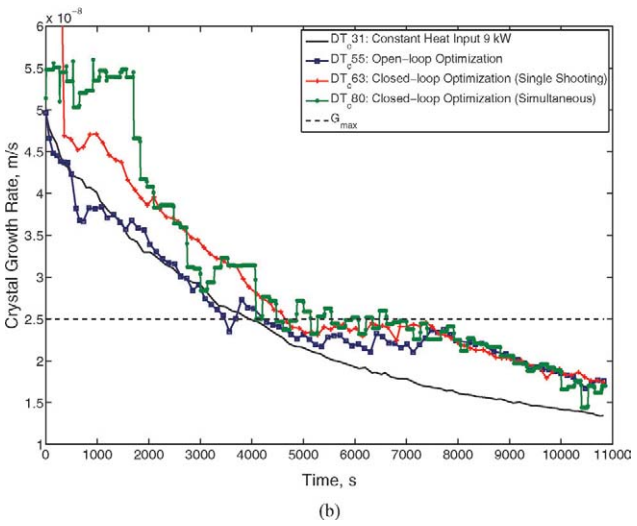


**Figure 6. Results of the open-loop and closed-loop control experiments.**

(a) Heat input profiles and (b) crystal growth rate profiles. [Color figure can be viewed in the online issue, which is available at wileyonlinelibrary.com.]

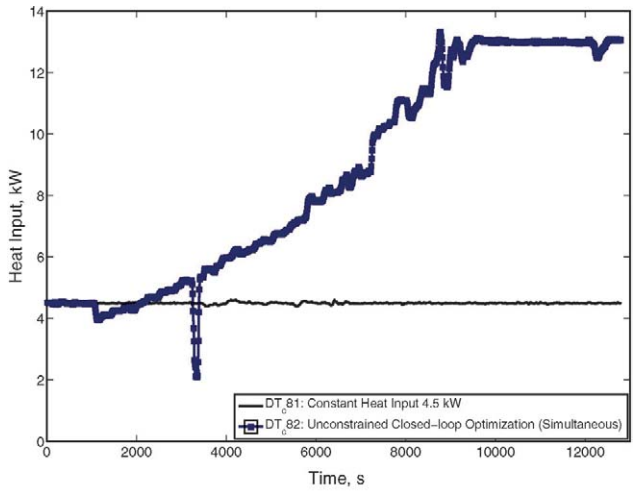


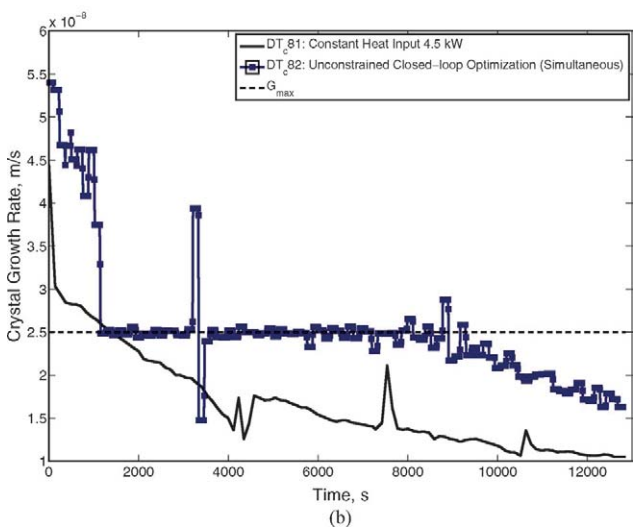


**Figure 7. Results of the closed-loop control experiment in the case of unconstrained optimization.**

(a) Heat input profiles and (b) crystal growth rate profiles. [Color figure can be viewed in the online issue, which is available at wileyonlinelibrary.com.]

differences in initial crystal growth rates of various batch runs are due to the different initial supersaturation levels at the seeding point; see Table 5.

Figure 6 indicates that optimal process operation cannot be achieved at all times during a batch run. The reference trajectory is violated at the beginning and toward the end of a batch run due to actuation limitations. The heat input is not lowered below 9.0 kW to avoid possible dissolution of seeds,[25] whereas the heat transfer constraints limit the heat input to an upper bound of 13 kW. The effect of the lower heat input bound on seed dissolution is investigated in experiment $DT_c81$, where the seeds are inserted into the crystallizer at the heat input of 4.5 kW. As shown in Figure

**Table 5. Description of the Seeded Fed-Batch Evaporative Crystallization Experiments**

| | Operating Conditions | | | | Seeding Conditions | |
|---|---|---|---|---|---|---|
| Experiment | Temperature (°C) | Pressure (mbar) | Impeller Frequency (rpm) | Heat input (kW) | Seed aging time (min) | Initial Supersaturation |
| $DT_c31$ | 50 | 100 | 450 | 9.0 | 57 | 0.01627 |
| $DT_c55$ | 50 | 100 | 450 | Figure 6a | 60 | 0.00567 |
| $DT_c63$ | 50 | 100 | 450 | Figure 6a | 59 | 0.00718 |
| $DT_c80$ | 50 | 100 | 450 | Figure 6a | 53 | 0.01103 |
| $DT_c81$ | 50 | 100 | 450 | 4.5 | 55 | 0.00705 |
| $DT_c82$ | 50 | 100 | 450 | Figure 7a | 62 | 0.00683 |

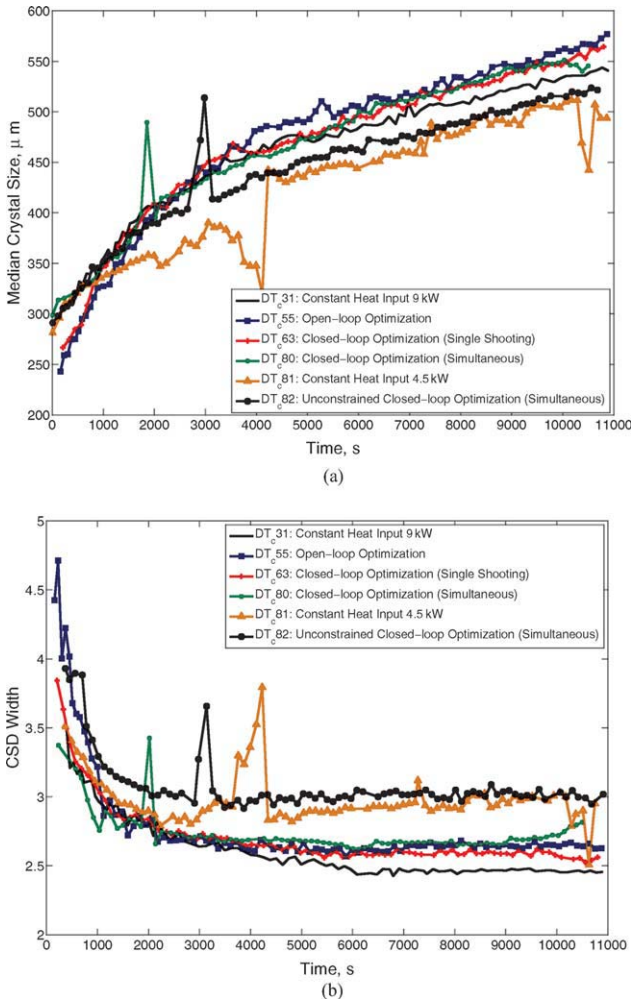


**Figure 8. The evolution of median and width of the crystal size distribution throughout the batch experiments.**

(a) Median crystal size and (b) width of the crystal size distribution. [Color figure can be viewed in the online issue, which is available at wileyonlinelibrary.com.]

7, the heat input is kept constant throughout the batch run, resulting in a continuous violation of the maximum crystal growth rate. The on-line CSD measurements suggest that the CSD attributes of the first measurement taken immediately after seeding remain to a large extent similar to those obtained in experiment $DT_c31$; see Figure 8. Therefore, it is unlikely that the seeds dissolve when they are exposed to lower heat inputs than 9 kW.

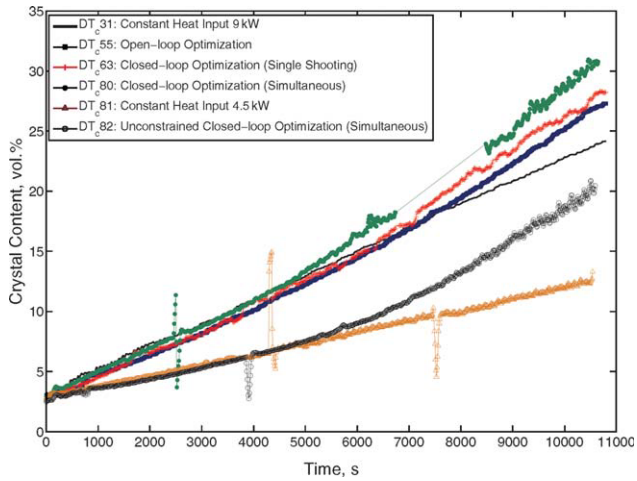


**Figure 9. The evolution of batch crystal content throughout the experiments.**

[Color figure can be viewed in the online issue, which is available at wileyonlinelibrary.com.]

The lower heat input bound of the optimal control problem is decreased to 2 kW in experiment $DT_c82$. In this batch run, the seeds are inserted into the crystallizer at the heat input of 4.5 kW. The controller is switched on after obtaining 8 reliable CSD measurements in order to properly initialize the simultaneous dynamic optimizer. It is observed in Figure 7a that the heat input is readily reduced to 3.9 kW to bring the crystal growth rate to the reference trajectory, i.e., $G_{max}$. Subsequently, a good reference trajectory tracking is achieved till the heat input reaches its upper bound of 13 kW. Figure 7b indicates that the control approach enables effective crystal growth rate control until the lack of process actuation hinders the optimal operation toward the batch end.

The evolution of crystal volume content of various batch runs is depicted in Figure 9. The spikes in the crystal content measurements are due to regular rinsing of the product line of the crystallizer to prevent blockage. It is evident that the application of the control approach leads to a substantial increase, i.e., up to 30%, in productivity in comparison with batch runs with constant heat input; see Table 6. The larger crystal content at the end of the controlled batch runs is due to the higher crystal growth rates. It is observed that the dynamic optimizers yield almost the same productivity, though the simultaneous dynamic optimizer results in a slightly higher crystal content at the batch end. Figure 9 suggests that the optimal crystal growth rate profile in experiment $DT_c82$ is obtained at the expense of reduced batch

**Table 6. Results of the Batch Runs in the 75-l Draft Tube Crystallizer**

| Experiment | Control Approach | Optimization Strategy | Results at the Batch End (10800 s) | | |
|---|---|---|---|---|---|
| | | | Crystal Content (vol. %) | Median Crystal Size ($\mu$ m) | CSD Width |
| $DT_c31$ | – | – | 24.2 | 544 | 2.45 |
| $DT_c55$ | Open-loop | Single shooting | 27.3 | 573 | 2.62 |
| $DT_c63$ | Closed-loop | Single shooting | 28.3 | 565 | 2.56 |
| $DT_c80$ | Closed-loop | Simultaneous | 30.8 | 546 | 2.82 |
| $DT_c81$ | – | – | 12.9 | 512 | 2.80 |
| $DT_c82$ | Closed-loop | Simultaneous | 20.0 | 521 | 3.02 |

productivity. This results from the lower crystal growth rates at the beginning of experiment $DT_c82$. Clearly, achieving the desired product quality requirements attained by effective crystal growth rate control is of greater significance than maximizing the batch productivity.

The results of on-line CSD measurements shown in Figure 8 suggest that the start-up phase of the batch runs is to a large extent reproducible. This is due to the optimal seeding procedure that largely circumvents uncertain initial conditions. Figure 8 indicates that the CSD attributes of the product crystals remain almost similar. However, reducing the lower heat input bound results in somewhat smaller crystals due to the lower crystal growth rates at the beginning of the batch run; see Table 6. The broader CSD width in experiments $DT_c81$ and $DT_c82$ is attributed to the lower initial supersaturation levels as listed in Table 5. Low-initial supersaturation may cause partial dissolution of seeds, leading to product quality degradation.

## Conclusions

This paper demonstrates real-time implementation of a model-based control approach on a semi-industrial batch crystallizer. The on-line computation of the underlying optimal control problem by means of different direct optimization strategies is thoroughly examined. The optimal control problem aims to maximize the batch productivity by attaining a maximum admissible crystal growth rate at all times during a batch run. The maximum crystal growth rate circumvents product quality degradation arisen from excessively high supersaturation. An extended Luenberger-type observer is developed to facilitate closed-loop application of the control approach. In addition, the observer provides estimations for the unmeasured process variable, namely, the solute concentration, by using the nonlinear moment model and on-line CSD measurements. Real-time implementations of the control approach indicate that on-line computation of the optimal operating policy outperforms open-loop implementation of the off-line optimized profiles. This is due to the state estimation in the feedback control system, which largely accounts for model imperfections and process uncertainties. The experimental results suggest that the control approach leads to a substantial increase in the batch productivity, as sustaining the product quality.

The optimal control problem is solved by various direct optimization strategies, namely, single shooting, multiple shooting, and simultaneous strategies. The simulation and experimental results indicate that the optimization strategies hardly differ in terms of optimal operation of the crystallizer at hand. However, the single shooting strategy has a much higher computational burden. The multiple shooting and simultaneous strategies are expected to better suit on-line optimization of industrial batch crystallizers represented by full population balance models. The thorough analysis of the direct optimization strategies provided in this paper will pave the way for real-time control of a wide range of industrial batch crystallization processes.

## Acknowledgments

The work presented in this article was carried out within the EUREKA/IS-project E! 3458/IS043074, called CryPTO (Crystallizer based Processing: fundamenTal research into mOdelling). The financial support of SenterNovem is gratefully acknowledged. The authors thank Jeffrey Landlust for his assistance in real-time implementation of the control approach.

## Literature Cited

1. Braatz RD. Advanced control of crystallization processes. *Ann Rev Control*. 2002;26:87–99.
2. Huesman A, Van den Hof P, Stankiewicz A. On the essential role of process control in process intensification. In: *Proceedings of the 2nd European Process Intensification Conference*, Venice, Italy, 2009.
3. Mullin JW, Nyvlt J. Programmed cooling of batch crystallizers. *Chem Eng Sci*. 1971;26:369–377.
4. Jones AG, Mullin JW. Programmed cooling crystallization of potassium sulphate solutions. *Chem Eng Sci*. 1974;29:105–118.
5. Mayrhofer B, Nyvlt J. Programmed cooling of batch crystallizations. *Chem Eng Process*. 1988;24:217–220.
6. Jones AG. Optimal operation of a batch cooling crystallizer. *Chem Eng Sc*. 1974;29:1075–1087.
7. Chang CT, Epstein MAF. Identification of batch crystallization control strategies using characteristic curves. *AIChE Symp Ser*. 1982;78:68–75.
8. Rawlings JB, Miller SM, Witkowski WR. Model identification and control of solution crystallization processes: A review. *Ind Eng Chem Res*. 1993;32:1275–1296.
9. Matthews HB, Rawlings JB. Batch crystallization of a photochemical: Modeling, control and filtration. *AIChE J*. 1998;44:1119–1127.
10. Lang YD, Cervantes AM, Biegler LT. Dynamic optimization of a batch cooling crystallization process. *Ind Eng Chem Res*. 1999;38:1469–1477.
11. Chung SH, Ma DL, Braatz RD. Optimal seeding in batch crystallization. *Can J Chem Eng*. 1999;77:590–596.
12. Ma DL, Chung SH, Braatz RD. Worst-case performance analysis of optimal batch control trajectories. *AIChE J*. 1999;45:1469–1476.
13. Ma DL, Tafti DK, Braatz RD. Optimal control and simulation of multidimensional crystallization process. *Comput Chem Eng*. 2002;26:1103–1116.
14. Nagy ZK, Braatz RD. Open-loop and closed-loop robust optimal control of batch processes using distributional and worst-case analysis. *J Process Control*. 2004;14:411–422.
15. Hu Q, Rohani S, Wang DX, Jutan A. Optimal control of a batch cooling seeded crystallizer. *Powder Technol*. 2005;156:170–176.
16. Nowee SM, Abbas A, Romagnoli JA. Optimization in seeded cooling crystallization: A parameter estimation and dynamic optimization study. *Chem Eng Process*. 2007;46:1096–1106.
17. Chang CT, Epstein MAF. Simulation studies of a feedback control strategy for batch crystallizers. *AIChE Symp Ser*. 1987;83:110–119.
18. Eaton JW, Rawlings JB. Feedback control of chemical processes using online optimization techniques. *Comput Chem Eng*. 1990;14:469–479.
19. Zhang GP, Rohani S. Online optimal control of a seeded batch cooling crystallizer. *Chem Eng Sci*. 2003;58:1887–1896.
20. Abbas A, Romagnoli JA. DCS implementation of optimal operational policies: a crystallisation case study. *Int J Comput Appl Technol*. 2006;25:198–208.
21. Sheikhzadeh M, Trifkovic M, Rohani S. Real-time optimal control of an anti-solvent isothermal semi-batch crystallization process. *Chem Eng Sci*. 2007;63:829–839.
22. Landlust J, Mesbah A, Wildenberg J, Kalbasenka AN, Kramer HJM, Ludlage JHA. An industrial model predictive control architecture for batch crystallization. In: *Proceedings of the 17th International Symposium on Industrial Crystallization*, Maastricht, The Netherlands, 2008:35–42.
23. Nagy ZK. Model based robust control approach for batch crystallization product design. *Comput Chem Eng*. 2009;33:1685–1691.
24. Fujiwara M, Nagy ZK, Chew JW, Braatz RD. First-principles and direct design approaches for the control of pharmaceutical crystallization. *J Process Control*. 2005;15:493–504.
25. Kalbasenka AN, Spierings L, Huesman AEM, Kramer HJM. Application of seeding as a process actuator in a model predictive control framework for fed-batch crystallization of ammonium sulphate. *Part Part Syst Char*. 2007;24:40–48.
26. Hulbert HM, Katz S. Some problems in particle technology: A statistical mechanical formulation. *Chem Eng Sc*. 1964;9:555–574.

27. Randolph AD, Larson MA. *Theory of Particulate Processes*, 2nd ed. San Diego: Academic Press, 1988.
28. Daudey PJ, van Rosmalen GM, De Jong EI. Secondary nucleation kinetics of ammonium sulphate in a cmsmpr crystallizer. *J Crys Growth*. 1990;99:1076–1081.
29. Mesbah A, Landlust J, Huesman AEM, Kramer HJM, Jansens PJ, Van den Hof PMJ. A model-based control framework for industrial batch crystallization processes. *Chem Eng Res Design*. doi:10.1016/j.cherd.2009.09.010.
30. Doki N, Kubota N, Yokota M, Chianese A. Determination of critical seed loading ratio for the production of crystals of uni-modal size distribution in batch cooling crystallization of potassium alum. *J Chem Eng Jpn*. 2002;35:670–676.
31. Fujiwara M, Shan Chow p, Ma DL, Braatz RD. Paracetamol crystallization using laser backscattering and ATR-FTIR spectroscopy: Metastability, agglomeration and control. *Cryst Growth Des*. 2002;2:363–370.
32. Simon LL, Nagy ZK, Hungerbuhler K. Endoscopy-based in situ bulk video imaging of batch crystallization processes. *Org Process Res Dev*. 2009;13:1254–1261.
33. Simon LL, Nagy ZK, Hungerbuhler K. Comparison of external bulk video imaging with focused beam reflectance measurement and ultra-violet visible spectroscopy for metastable zone identification in food and pharmaceutical crystallization processes. *Chem Eng Sci*. 2009;64:3344–3351.
34. Kalbasenka AN, Huesman AEM, Kramer HJM, Bosgra OH. Controllability analysis of industrial crystallizers. In: *Proceedings of the 12th International Workshop on Industrial Crystallization*, Halle (Saale), Germany, 2005:157–164.
35. Keerthi SS, Gilbert EG. Optimal infinite-horizon feedback laws for a general class of constrained discrete-time systems: Stability and moving-horizon approximations. *J Optim Theory Appl*. 1988;57:265–293.
36. Biegler LT, Cuthrell JE. Improved infeasible path optimization for sequential modular simulators II: The optimization algorithm. *Comput Chem Eng*. 1985;9:257–267.
37. Cuthrell JE, Biegler LT. Simultaneous optimization and solution methods for batch reactor control profiles. *Comput Chem Eng*. 1989;13:49–62.
38. Bock HG, Plitt K. A multiple shooting algorithm for direct solution of optimal control problems. In: *Proceedings of the 9th IFAC World Congress*, Budapest, Hungary, 1984.
39. Diehl M, Bock HG, Schloder JP, Findeisen R, Nagy ZK, Allgower F. Real-time optimization and nonlinear model predictive control of processes governed by differential-algebraic equations. *J Process Control*. 2002;12:577–585.
40. Huesman AEM, Bosgra OH, Van den Hof PMJ. Degrees of freedom analysis of economic dynamic optimal plantwide operation. In: *Proceedings of the 8th International IFAC Symposium on Dynamics and Control of Process Systems*, Cancun, Mexico, 2007:165–170.
41. Nagy ZK, Allgower F, Franke R, Frick A, Mahn B. Efficient tool for nonlinear model predictive control of batch processes. In: *Proceedings of the 12th Mediterranean Conference on Control and Automation*, Kusadasi, Turkey, 2004.
42. Simon LL, Kencse H, Hungerbuhler K. Optimal rectification column, reboiler vessel, connection pipe selection and optimal control of batch distillation considering hydraulic limitations. *Chem Eng Process*. 2009;48:938–949.
43. Simon LL, Nagy ZK, Hungerbuhler K. Model based control of a liquid swelling constrained batch reactor subject to recipe uncertainties. *Chem Eng J*. 2009;153:151–158.
44. Franke R, Arnold E, Linke H. HQP: A solver for nonlinearly constrained optimization. 2005, Available at: http://hqp.sourceforge.net, May 10, 2010.
45. Brown PN, Hindmarsh AC, Petzold LR. Using krylov methods in the solution of large-scale differential algebraic systems. *SIAM J Sci Comput*. 1994;15:1467–1488.
46. Hermanto MW, Chiu MS, Braatz RD. Nonlinear model predictive control for the polymorphic transformation of L-glutamic acid crystals. *AIChE J*. 2009;55:2631–2645.
47. Ciccarella G, Dalla Mora M, Germani A. A luenberger-like observer for nonlinear systems. *Int J Control*. 1993;57:537–556.
48. Kalbasenka AN, Landlust J, Huesman AEM, Kramer HJM. Application of observation techniques in a model predictive control framework of fed-batch crystallization of ammonium sulphate. In: *Proceedings of AIChE Spring Meeting*, volume 2, Orlando, FL, USA, 2006:227.

*Manuscript received Nov. 2, 2009, revision received Apr. 28, 2010, and final revision received June 30, 2010.*